- Difference in Screening Effect of Alkali Metal Counterions on H-AOT-Based W/O Microemulsion Formation
  Oshitani, J.; Takashina, S.; Yoshida M.; Gotoh, K. *Langmuir* **2010**, *26*, 2274–2278.
  Abstract:

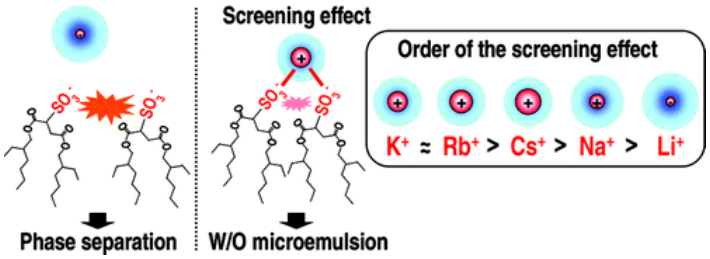

The purpose of this study was to estimate the screening of electrostatic repulsions between the polar headgroups of AOT^- by alkali metal counterions and to explore the relationships between the screening effect and the phase behavior of H-AOT-based W/O microemulsions. The screening effect was evaluated by means of critical micelle concentration (CMC) data using the pyrene 1:3 ratio method with aqueous solutions containing M-AOT (where M^+ = Li^+, Na^+, K^+, Rb^+ and Cs^+) to form normal micelles, and by counterion binding constants, determined from plots of CMC versus counterion concentration. The order of the screening effect was found to be $K^+ \approx Rb^+ > Cs^+ > Na^+ > Li^+$. Interestingly, the order does not follow the hydration size dependence of the alkali metal counterions. An aqueous MOH solution containing a given concentration/H-AOT/isooctane was emulsified at a water content (w_0 = [water]/[H-AOT]) of 10 to produce H-AOT-based W/O microemulsions. The phase behavior and size variation were investigated by FT-IR and DLS measurements. The emulsified mixture separates into two phases at lower MOH concentration due to an insufficient screening effect. When the concentration is increased to a level sufficient to intensify the screening effect, W/O microemulsions are formed without phase separation at lower KOH and RbOH concentrations compared to CsOH. A period of standing after the emulsification and a higher concentration of NaOH compared to KOH, RbOH, and CsOH are required to form W/O microemulsions. W/O microemulsions are not formed in the case of LiOH. These results indicate that the formation of a W/O microemulsion with H-AOT is strongly correlated with the order of the screening effect. A possible cause for the difference in the screening effect is proposed based on hydration of the polar headgroups and counterions, as evidenced by FT-IR spectral data, i.e., symmetrical sulfonate stretching and O−H stretching.

- Interfacing Live Cells with Nanocarbon Substrates
  Agarwal, S.; Zhou, X.; Ye, F.; He, Q.; Chen, G. C. K.; Soo, J.; Boey, F.; Zhang, H.; Chen, P. *Langmuir* **2010**, *26*, 2244–2247.
  Abstract:

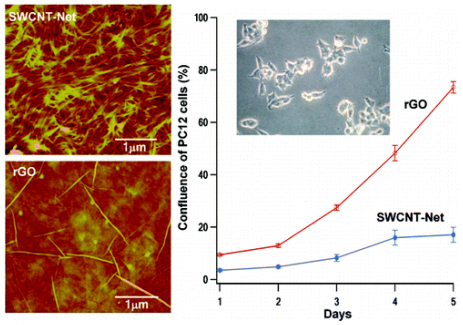

Nanocarbon materials, including single-walled carbon nanotubes (SWCNTs) and graphene, promise various novel biomedical applications (e.g., nanoelectronic biosensing). In this Letter, we study the ability of SWCNT networks and reduced graphene oxide (rGO) films in interfacing several types of cells, such as neuroendocrine PC12 cells, oligodendroglia cells, and osteoblasts. It was found that rGO is biocompatible with all these cell types, whereas the SWCNT network is inhibitory to the proliferation, viability, and neuritegenesis of PC12 cells, and the proliferation of osteoblasts. These observations could be attributed to the distinct nanotopographic features of these two kinds of nanocarbon substrates.

- Spontaneous Hierarchical Assembly of Crown Ether-like Macrocycles into Nanofibers and Microfibers Induced by Alkali-Metal and Ammonium Salts
  Hui, J. K.-H.; Frischmann, P. D.; Tso, C.-H.; Michal, C. A.; MacLachlan, M. J. *Chem. Eur. J.* **2010**, *16*, 2453-2460.
  Abstract:

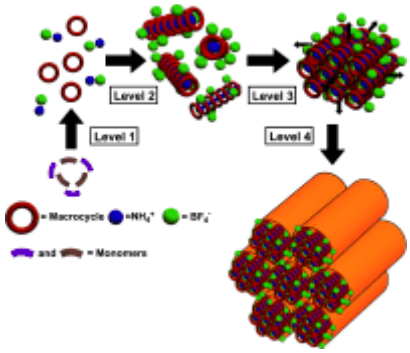

Schiff base macrocycle 1, which has a crown ether like central pore, was combined with different alkali-metal and ammonium salts in chloroform, resulting in one-dimensional supramolecular aggregates. The ion-induced self-assembly was studied with solid-state NMR spectroscopy, transmission electron microscopy (TEM), scanning electron microscopy (SEM), and atomic force microscopy (AFM). It was found that the lengths and widths of the superstructures depend on the cation and counteranion of the salts. Among the salts being used, Na^+ and NH_4^+ ions with BF_4^- ions showed the most impressive fibrous structures that can grow up to 1 μm in diameter and hundreds of microns in length. In addition, the size of the fibers can be controlled by the evaporation rate of the solvent. A new macrocycle with bulky triptycenyl substituents that prevent supramolecular assembly was prepared and did not display any nanofibers with alkali-metal ions in chloroform when studied with TEM.

- Combination of Cobalt and Iron Polypyridine Complexes for Improving the Charge Separation and Collection in Ru(terpyridine)$_2$-Sensitised Solar Cells
  Caramori, S.; Husson, J.; Beley, M.; Bignozzi, C. A.; Argazzi, R.; Gros, P. C. *Chem. Eur. J.* **2010**, *16*, 2611-2618.
  Abstract:

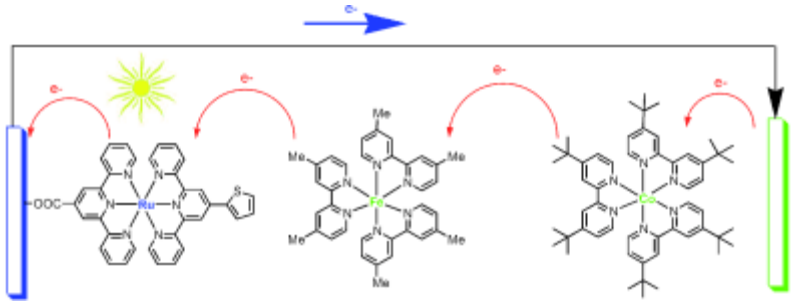

Mixtures of polypyridine Fe^{II} and Co^{II} complexes are used as electron mediators in Ru-thienyltpy-sensitised solar cells (tpy = terpyridine). The use of the metalorganic redox couples allows for improved charge-collection efficiency with respect to the classical iodide/iodine couple which, when associated to Ru-tpy_2 dyes, usually produces poor performance. The improved charge collection is explained by a combination of effective dye regeneration and decreased recombination with the oxidised electrolyte on the basis of data obtained by transient spectroscopy and photoelectrochemical measurements. The efficiency of the regeneration cascade is also critically dependent upon the ability of the Co^{II} complex to intercept Fe^{III} centres, as clearly indicated by chronocoulometry experiments.

- Tunable magnetic exchange interactions in manganese-doped inverted core–shell ZnSe–CdSe nanocrystals
  Bussian, D. A.; Crooker, S. A.; Yin, M.; Brynda, M.; Efros, A. L.; Klimov, V. I. *Nature Materials* **2009**, *8*, 35 - 40.
  Abstract:

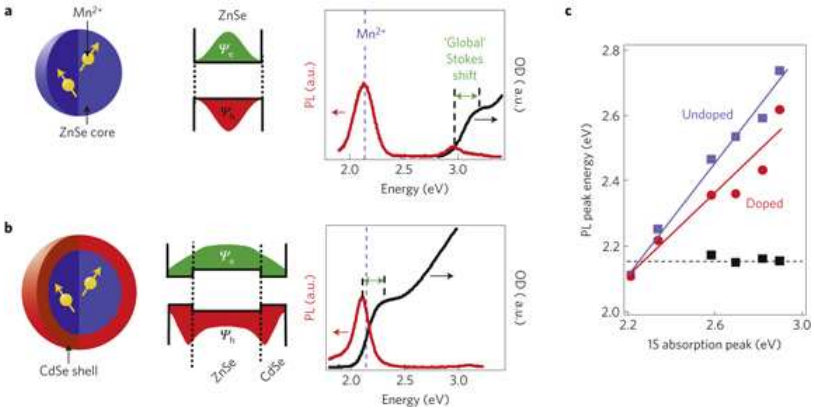

Magnetic doping of semiconductor nanostructures is actively pursued for applications in magnetic memory and spin-based electronics. Central to these efforts is a drive to control the interaction strength between carriers (electrons and holes) and the embedded magnetic atoms. In this respect, colloidal nanocrystal heterostructures provide great flexibility through growth-controlled 'engineering' of electron and hole wavefunctions in individual nanocrystals. Here, we demonstrate a widely tunable magnetic *sp–d* exchange interaction between electron–hole excitations (excitons) and paramagnetic manganese ions using 'inverted' core–shell nanocrystals composed of Mn^{2+}-doped ZnSe cores overcoated with undoped shells of narrower-gap CdSe. Magnetic circular dichroism studies reveal giant Zeeman spin splittings of the band-edge exciton that, surprisingly, are tunable in both magnitude and sign. Effective exciton *g*-factors are controllably tuned from -200 to +30 solely by increasing the CdSe shell thickness, demonstrating that strong quantum confinement and wavefunction engineering in heterostructured nanocrystal materials can be used to manipulate carrier–Mn^{2+} wavefunction overlap and the *sp–d* exchange parameters themselves.

- Regular arrays of highly ordered ferroelectric polymer nanostructures for non-volatile low-voltage memories
  Hu, Z.; Tian, M.; Nysten, B.; Jonas, A. M. *Nature Materials* **2009**, *8*, 62 – 67.
  Abstract:

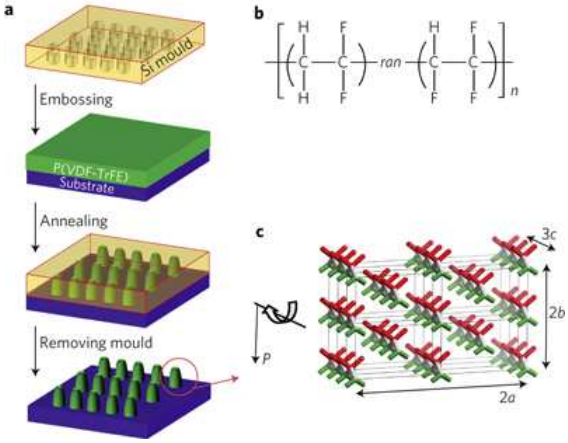

Ferroelectric nanostructures are attracting tremendous interest because they offer a promising route to novel integrated electronic devices such as non-volatile memories and probe-based mass data storage. Here, we demonstrate that high-density arrays of nanostructures of a ferroelectric polymer can be easily fabricated by a simple nano-embossing protocol, with integration densities larger than 33 Gbits inch^{-2}. The orientation of the polarization axis, about which the dipole moment rotates, is simultaneously aligned in plane over the whole patterned region. Internal structural defects are significantly eliminated in the nanostructures. The improved crystal orientation and quality enable well-defined uniform switching behaviour from cell to cell. Each nanocell shows a narrow and almost ideal square-shaped hysteresis curve, with low energy losses and a coercive field of ~10 MV m^{-1}, well below previously reported bulk values. These results pave the way to the fabrication of soft plastic memories compatible with all-organic electronics and low-power information technology.

- PEGylated polymers for medicine: from conjugation to self-assembled systems
  Joralemon, M. J.; McRae, S.; Emrick, T. *Chem. Commun.* **2010**, *46*, 1377 – 1393.
  Abstract :

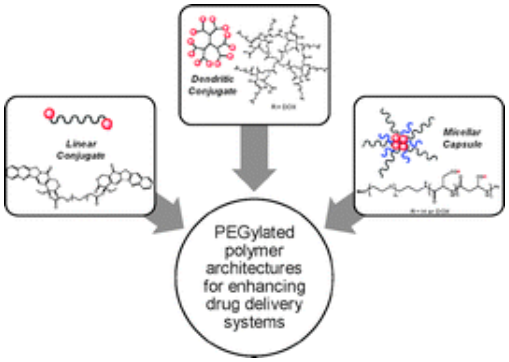

Synthetic polymers have transformed society in many areas of science and technology, including recent breakthroughs in medicine. Synthetic polymers now offer unique and versatile platforms for drug delivery, as they can be bio-tailored for applications as implants, medical devices, and injectable polymer-drug conjugates. However, while several currently used therapeutic proteins and small molecule drugs have benefited from synthetic polymers, the full potential of polymer-based drug

delivery platforms has not yet been realized. This review examines both general advantages and specific cases of synthetic polymers in drug delivery, focusing on PEGylation in the context of polymer architecture, self-assembly, and conjugation techniques that show considerable effectiveness and/or potential in therapeutics.

- Self-assembly of coordination polymers into multi-stranded nanofibers with tunable chirality
  Kim, H. J.; Kim, J. K.; Lee, M. *Chem. Commun.* **2010**, *46*, 1458 – 1460.
  Abstract:

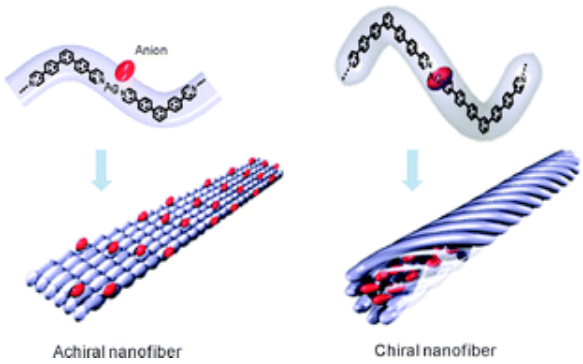

We have demonstrated that the formation of multi-stranded nanofibers with tunable chirality from coordination polymers and their hierarchical assembly into interconnected 3-D networks leading to thermoresponsive gelation.

- Monitoring Self-Sorting by Electrospray Ionization Mass Spectrometry: Formation Intermediates and Error-Correction during the Self-Assembly of Multiply Threaded Pseudorotaxanes
  Jiang, W.; Schäfer, A.; Mohr, P. C.; Schalley, C. A. *J. Am. Chem. Soc.* **2010**, *132*, 2309–2320.
  Abstract:

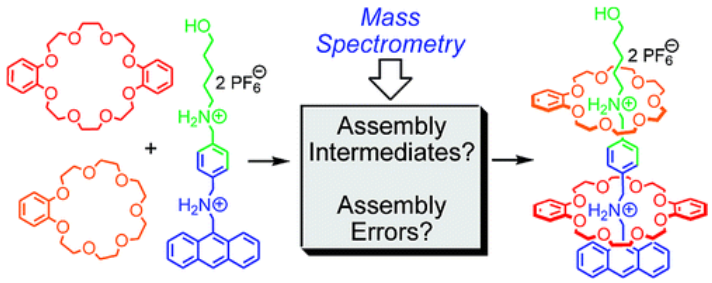

Three binary pseudorotaxanes, which are based on two different secondary ammonium/crown ether binding motifs, have been studied by 1H NMR and 1H,1H EXSY NMR experiments with respect to their thermodynamic stabilities and their axle exchange kinetics. The stability ranking does not follow the order of axle exchange rates, and the thermodynamically most stable axle−wheel combinations assemble only slowly. On the basis of these binding motifs, a series of self-sorting systems have been studied ranging from simple four-component mixtures through sequence-specific pseudorotaxanes to multiply threaded complexes. Because of the mismatch of kinetic and thermodynamic order, wrongly assembled structures are unavoidable, which require error-correction steps to yield the final thermodynamically controlled self-sorted products. These error-correction steps can easily be monitored by electrospray mass spectrometry, when a mixed-flow microreactor is coupled to the ion source to cover second time scales. Self-assembly intermediates, wrongly assembled structures, and the final thermodynamic products can be simultaneously identified. The determination of preferred

assembly pathways as well as the formation of dead-end structures provides a clear picture of a rich kinetic behavior of the self-sorting systems under study.

- Photoinitiated Growth of Sub-7 nm Silver Nanowires within a Chemically Active Organic Nanotubular Template
  Eisele, D. M.; Berlepsch, H.; Böttcher, C.; Stevenson, K. J.; Bout, D. A. V.; Kirstein, S.; Rabe, J. P. *J. Am. Chem. Soc.* **2009**, *131*, 2104–2105.
  Abstract:

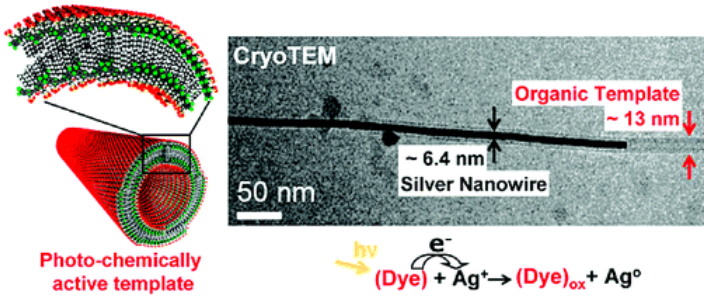

Self-assembled supramolecular nanotubes of J-aggregated amphiphilic cyanine dye in aqueous solution are employed as chemically active templates for the photoinitiated formation of silver nanowires with a very small and homogeneous diameter of (6.4 ± 0.5) nm. Key features of the template are (1) its small and well-defined diameter; (2) its photochemical activity, which allows photoinitiation of the structure formation; and (3) the processability in aqueous solution. The latter includes the potential to remove the template after the reaction, or to functionalize it further, e.g. with optoelectronically active polycations, providing access to quasi one-dimensional hybrid structures with well-defined metallic nanowires as a core.

- Substrate Catalysis Enhances Single-Enzyme Diffusion
  Muddana, H. S.; Sengupta, S.; Mallouk, T. E.; Sen, A.; Butler, P. J. *J. Am. Chem. Soc.* **2010**, *132*, 2110–2111.
  Abstract:

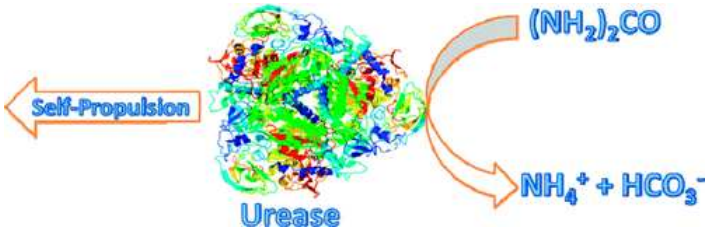

We show that diffusion of single urease enzyme molecules increases in the presence of urea in a concentration-dependent manner and calculate the force responsible for this increase. Urease diffusion measured using fluorescence correlation spectroscopy increased by 16−28% over buffer controls at urea concentrations ranging from 0.001 to 1 M. This increase was significantly attenuated when urease was inhibited with pyrocatechol, demonstrating that the increase in diffusion was the result of enzyme catalysis of urea. Local molecular pH changes as measured using the pH-dependent fluorescence lifetime of SNARF-1 conjugated to urease were not sufficient to explain the increase in diffusion. Thus, a force generated by self-electrophoresis remains the most plausible explanation. This force, evaluated using Brownian dynamics simulations, was 12 pN per reaction turnover. These measurements demonstrate force generation by a single enzyme molecule and lay the foundation

for a further understanding of biological force generation and the development of enzyme-driven nanomotors.

- Polymorphism and Reversible Mechanochromic Luminescence for Solid-State Difluoroboron Avobenzone
  Zhang, G.; Lu, J.; Sabat, M.; Fraser, C. L. *J. Am. Chem. Soc.* **2010**, *132*, 2160–2162.
  Abstract:

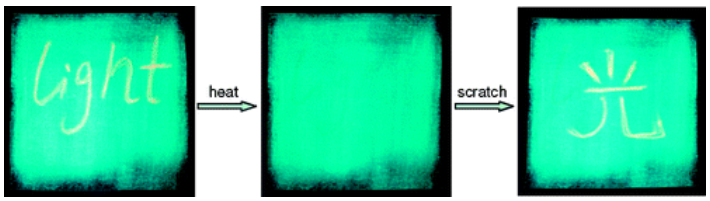

Difluoroboron avobenzone (BF_2AVB), a simple boron complex of a commercial sunscreen product, exhibits morphology-dependent emission and mechanochromic luminescence in the solid state. When scratched, smeared, or even gently touched, the emission color of BF_2AVB films is significantly red-shifted under UV excitation. In the rubbed regions, the fluorescence recovers slowly at room temperature or much faster with heating, resulting in a simple rewritable “scratch the surface” ink of potential commercial use.

- Single-Molecule Redox Blinking of Perylene Diimide Derivatives in Water
  Cordes, T.; Vogelsang, J.; Anaya, M.; Spagnuolo, C.; Gietl, A.; Summerer, W.; Herrmann, A.; Müllen, K.; Tinnefeld, P. *J. Am. Chem. Soc.* **2010**, *132*, 2404–2409.
  Abstract:

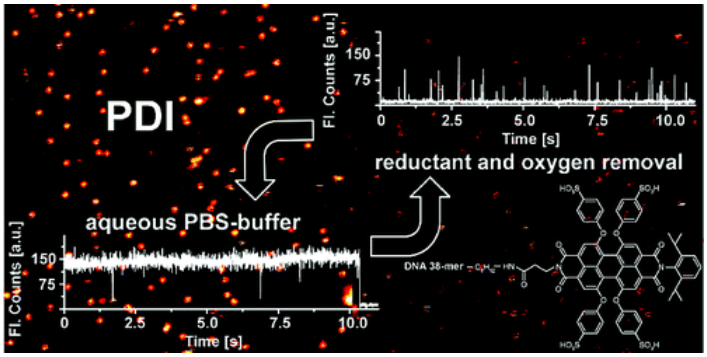

Dynamic developments in ultrasensitive and superresolution fluorescence microscopy call for improved fluorescence markers with increased photostability and new functionalities. We used single-molecule spectroscopy to study water-soluble perylene dicarboximide fluorophores (PDI), which were immobilized in aqueous buffer by attaching the fluorophore to DNA. Under these conditions bright fluorescence, comparable to that of single-molecule compatible organic fluorophores, is observed with homogeneous spectral and fluorescence decay time distributions. We additionally show how the fluorescence of the PDI can be controlled through photoinduced electron-transfer reactions by using different concentrations of reductants and oxidants, yielding either blinking or stable emission. We explain these properties by the redox potentials of PDI and the recently introduced ROXS (reducing and oxidizing system) concept. Finally, we evaluate how this fluorescence control of PDIs can be used for superresolution “Blink-Microscopy” in aqueous or organic media and more generally for single-molecule spectroscopy.

- Synthesis and Identification of a Trimethylenemethane Derivative π-Extended with Three Pyridinyl Radicals
  Matsumoto, K.; Inokuchi, D.; Hirao, Y.; Kurata, H.; Sato, K.; Takui, T.; Kubo, T. *Org. Lett.* **2010**, *12*, 836–839.
  Abstract:

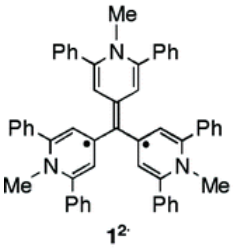

$1^{2\cdot}$
stable TMM derivative

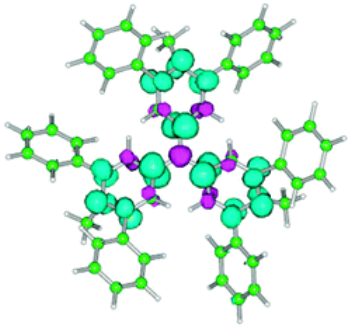

Spin density distribution of $1^{2\cdot}$

A trimethylenemethane (TMM) derivative $1^{2\bullet}$, in which the parent TMM is π-extended by the symmetric insertion of three pyridine rings into the C–C bonds of TMM, has been synthesized by the alkali metal reduction of the isolated corresponding dication. Although the frozen-glass X-band cw-ESR spectrum of $1^{2\bullet}$ gave unresolved fine structures due to the small ZFS parameters, pulsed ESR two-dimensional electron spin transient nutation (2D-ESTN) spectroscopy unambiguously can afford to identify diradical $1^{2\bullet}$ as a triplet species.

- Phosphaalkenes in π-Conjugation with Acetylenic Arenes
  Geng, X.-L.; Hu, Q.; Schäfer, B.; Ott, S. *Org. Lett.* **2010**, *12*, 692–695.
  Abstract:

Phosphaalkene inclusion at the periphery of acetylenic arenes results in decreased band gaps of the title compounds as verified by spectroscopic and electrochemical techniques. The electronic coupling between two 1-phosphahex-1-ene-3,5-diyne units is mediated by all *para*-substituted arenes and increases from **4b** to **4d**.

- Formation of Side-Chain Hetero-Polypseudorotaxane Composed of α- and β-Cyclodextrins with a Water-Soluble Polymer Bearing Two Recognition Sites
  Taura, D.; Li, S.; Hashidzume, A.; Harada, A. *Macromolecules* **2010**, *43*, 1706–1713.
  Abstract:

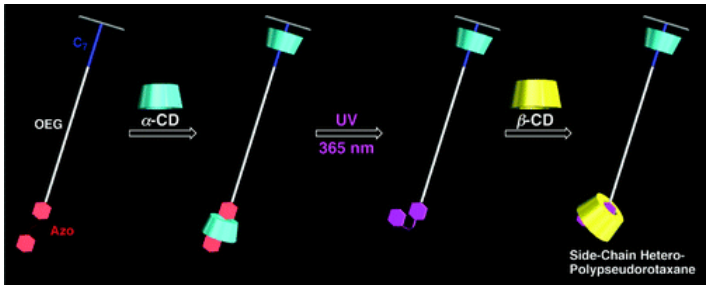

A side-chain hetero-polypseudorotaxane was prepared from a water-soluble polymer (**1**) bearing heptamethylene (C_7) and azobenzene (Azo) moieties connected with oligo(ethylene glycol) in the side chain by three steps, in which α- and β-cyclodextrins (α- and β-CDs) included the C_7 and *cis*-Azo moieties, respectively. In the first step, α-CD was added to **1** to form the side-chain polypseudorotaxane, in which α-CD included both the C_7 and *trans*-Azo moieties in the side chain. In the second step, the Azo moiety at the end of the side chain was isomerized to the *cis* isomer to form the side-chain polyrotaxane, in which α-CD was interlocked on the side chain. In the final step, β-CD was added to the side-chain polyrotaxane to form the side-chain hetero-polypseudorotaxane.

- Ring-Opening Metathesis Block Copolymerization of Amino Acid Functionalized Norbornene Monomers. Effects of Solvent and pH on Micelle Formation
  Sutthasupa, S.; Shiotsuki, M.; Matsuoka, H.; Masuda, T.; Sanda, F. *Macromolecules* **2010**, *43*, 1815–1822.
  Abstract:

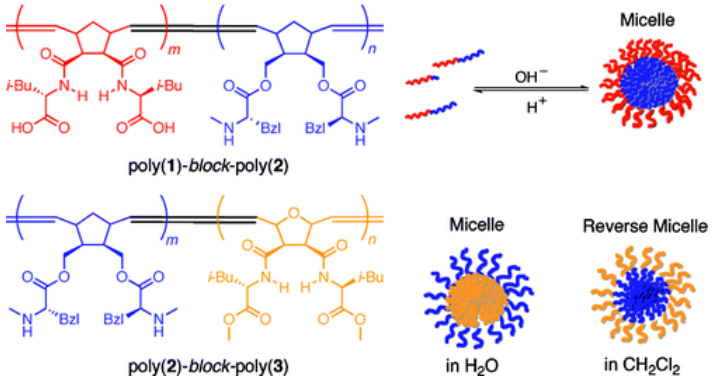

Amino acid derived norbornene monomers having unprotected carboxy (**1**) and amino groups (**2**) and 7-oxanorbornene having ester groups (**3**) were block copolymerized using the Grubbs ruthenium complexes. In the combination of **1** and **2**, block copolymers with number-average molecular weights ranging from 43 000 to 95 000 were obtained in good yields. Poly(**1**)$_{75}$-*block*-poly(**2**)$_{25}$ was soluble in 0.5 M NaOH(aq) but insoluble in 0.1 M HCl, while poly(**1**)$_{25}$-*block*-poly(**2**)$_{75}$ was soluble in 0.1 M HCl but insoluble in 0.5 M NaOH(aq). Thus, the block compositions remarkably affected the solubility of the copolymers in acidic and basic media. On the other hand, poly(**2**)$_{62}$-*block*-poly(**3**)$_{38}$ was soluble in H_2O but insoluble in CH_2Cl_2 and $CHCl_3$, while poly(**2**)$_{38}$-*block*-poly(**3**)$_{62}$ was soluble in CH_2Cl_2 and $CHCl_3$ but insoluble in H_2O. In this monomer combination, the block compositions significantly affected the solubility of the copolymers in organic and aqueous media. ^{1}H NMR spectroscopic, turbidity, and dynamic light scattering measurements revealed that poly(**1**)$_{50}$-*block*-poly(**2**)$_{50}$ formed micelles with a diameter around 130 nm in 0.5 M NaOH(aq). In a similar manner, it was revealed that poly(**2**)$_{62}$-*block*-poly(**3**)$_{38}$ and poly(**2**)$_{38}$-*block*-poly(**3**)$_{62}$ formed micelles with a diameter around 80 nm in H_2O and reverse micelles with a diameter around 45 nm in CH_2Cl_2, respectively.

- Microfluidic stochastic confinement enhances analysis of rare cells by isolating cells and creating high density environments for control of diffusible signals
  Vincent, M. E.; Liu, W.; Haney, E. B.; Ismagilov, R. F. *Chem. Soc. Rev.* **2010**, *39*, 974 – 984.
  Abstract:

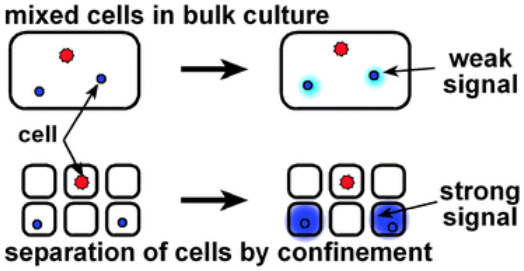

Rare cells can be difficult to analyze because they either occur in low numbers or coexist with a more abundant cell type, yet their detection is crucial for diagnosing disease and maintaining human health. In this *tutorial review*, we introduce the concept of microfluidic stochastic confinement for use in detection and analysis of rare cells. Stochastic confinement provides two advantages: (1) it separates rare single cells from the bulk mixture and (2) it allows signals to locally accumulate to a higher concentration around a single cell than in the bulk mixture. Microfluidics is an attractive method for implementing stochastic confinement because it provides simple handling of small volumes. We present technologies for microfluidic stochastic confinement that utilize both wells and droplets for the detection and analysis of single cells. We address how these microfluidic technologies have been used to observe new behavior, increase speed of detection, and enhance cultivation of rare cells. We discuss potential applications of microfluidic stochastic confinement to fields such as human diagnostics and environmental testing.

- Synthetic Routes to *meso*-Patterned Porphyrins
  Lindsey, J. S. *Acc. Chem. Res.* **2010**, *43*, 300–311.
  Abstract:

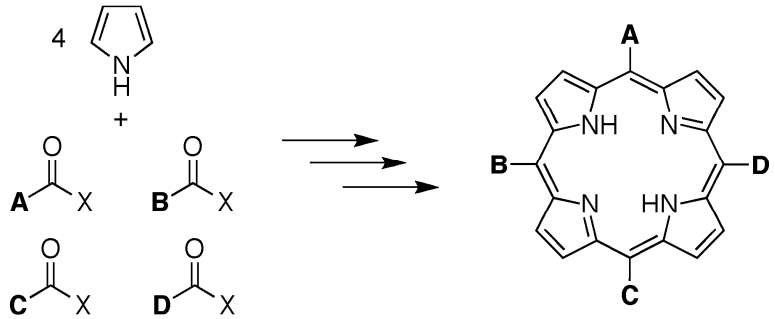

Synthetic *meso*-substituted porphyrins offer significant attractions compared with naturally occurring β-substituted porphyrins. The attractions include the rectilinear arrangement of the four *meso* substituents and potential synthetic amenability from pyrrole and simple acyl reactants, thereby avoiding the cumbersome syntheses of β-substituted pyrroles. In practice, however, the classical methods for the synthesis of *meso*-substituted porphyrins were characterized by high-temperature reactions, limited scope of substituents, and statistical mixtures accompanied by laborious chromatography if porphyrins bearing two different types of substituents were sought. Such methods left unrealized the tremendous utility of *meso*-substituted porphyrins across the enormously broad field of porphyrin science, which touches pure chemistry; energy, life and materials sciences; and medicine.

This Account surveys a set of strategies, developed over a generation, that provide rational access to porphyrins bearing up to four distinct *meso* substituents. A “2 + 2” route employs a dipyrromethane-1,9-dicarbinol and a dipyrromethane (bearing ABC- and D-substituents, respectively) in a two-step, one-flask process of acid-catalyzed condensation followed by oxidation at room temperature to form the free base “ABCD-porphyrin.” A “bilane” route relies on the acid-catalyzed reaction of a 1-

acyldipyrromethane (CD substituents) and a 9-bromodipyrromethane-1-carbinol (AB substituents) to form the corresponding 19-acyl-1-bromobilane. Reaction of the latter compound in the presence of $MgBr_2$, 1,8-diazabicyclo[5.4.0]undec-7-ene (DBU), and toluene at reflux exposed to air affords the corresponding magnesium(II) porphyrin. The two routes are complementary, both in scope and in implementation. A suite of methods also affords *trans*-A_2B_2-porphyrins by reaction of a dipyrromethane and an aldehyde, self-condensation of a dipyrromethane-1-carbinol, or self-condensation of a 1-acyldipyrromethane. These new routes are also useful for preparing sparsely substituted porphyrins, which bear fewer than four *meso* substituents (e.g., *trans*-AB-porphyrins, A-porphyrins). Because of their compact size and the ability to incorporate hydrophilic or amphipathic groups, such molecules are ideal for biological applications.
The success of these new synthetic strategies has relied on a number of advances including (1) the development of simple yet efficient routes to dipyrromethanes, acyldipyrromethanes, and dipyrromethane-carbinols, (2) the identification of acid catalysts and reaction conditions for condensations of pyrromethane species without accompanying acidolysis (which underlies scrambling and formation of a mixture of porphyrin products), (3) the development of analytical methods to rapidly screen for scrambling and to characterize the distribution of oligopyrromethanes and macrocycles, (4) selection and refinement of synthetic methods to increase yields and to limit or avoid use of chromatography, thereby achieving scalability to multigram levels, and (5) exploitation of discoveries concerning the fundamental chemistry of pyrrolic species. With these developments, the prior era of porphyrin synthesis has been supplanted with rational routes that proceed under very mild conditions and afford a single porphyrin bearing up to four distinct *meso* substituents. The *meso* substituents encompass a very wide range of molecular complexity. The resulting porphyrins can serve as building blocks in the construction of model systems, as components of molecular materials, and as surrogates for naturally occurring tetrapyrrole macrocycles.

- A facile route to ketene-functionalized polymers for general materials applications
  Leibfarth, F. A.; Kang, M.; Ham, M.; Kim, J.; Campos, L. M.; Gupta, N.; Moon, B.; Hawker, C. J. *Nature Chemistry* **2010**, *2*, 207-212.
  Abstract:

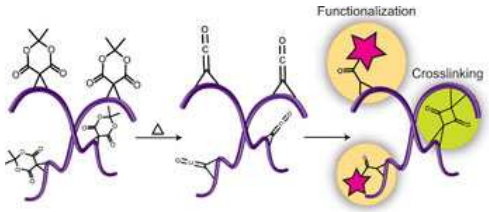

The ability to rapidly functionalize polymers is vital for application development. Here, a method for the introduction of masked ketenes into monomers for both ring-opening metathesis and radical-type polymerizations is described. These ketenes — a group previously underexploited in polymer chemistry — allow both crosslinking and post-polymerization functionalization of the polymers.

- Organocatalytic cascade reactions as a new tool in total synthesis
  Grondal, C.; Jeanty, M.; Enders, D. *Nature Chemistry* **2010**, *2*, 167-178.
  Abstract:

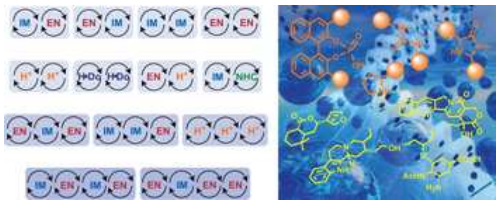

The field of organocatalysis has grown rapidly in the past decade to become, along with metal catalysis and biocatalysis, a third pillar of asymmetric catalysis. Here, progress in the use of organocatalytic cascade reactions for total synthesis is reviewed. The elegance and efficiency of such cascades mean that they have emerged as a powerful tool in synthetic organic chemistry.

- Supramolecular Assemblies Formed on an Epitaxial Graphene Superstructure
  Pollard, A. J.; Perkins, E. W.; Smith, N. A.; Saywell, A.; Goretzki, G.; Phillips, A. G.; Argent, S. P.; Sachdev, H.; Müller, F.; Hofner, S.; Gsell, S.; Fischer, M.; Schreck, M.; Osterwalder, J.; Greber, T.; Berner, S.; Champness, N. R.; Beton, P. H. *Angew. Chem. Int. Ed.* **2010**, *49*, 1794 –1799.
  Abstract:

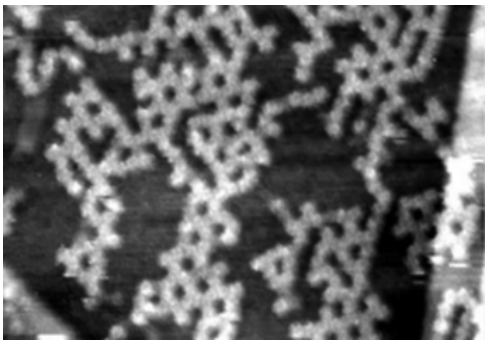

Quite comparable: A graphene monolayer is used as a substrate for the growth of two-dimensional hydrogen-bonded supramolecular structures (see STM image). The formation of these extended structures arises from a commensurability between their dimensions and a moiré pattern formed by the graphene.

- Photochromic Supramolecular Memory With Nondestructive Readout
  Karnbratt, J.; Hammarson, M.; Li, S.; Anderson, H. L.; Albinsson, B.; Andreasson, J. *Angew. Chem. Int. Ed*. **2010,** *49*, 1854 –1857.
  Abstract:

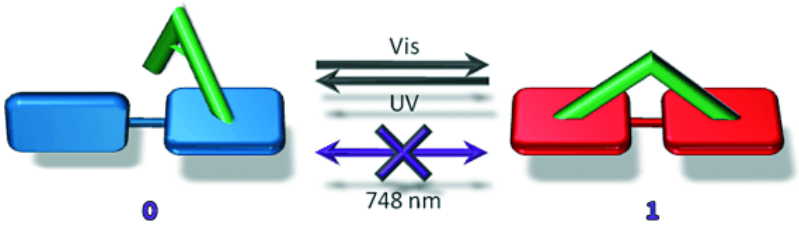

Looking without touching: The light-controlled isomerization of a complex containing a pyridine-appended dithienylethene (DTE; green) and a porphyrin dimer induces dramatic structural and spectral changes (see picture). These changes are monitored in a region outside the photochromically active absorption bands of DTE, therefore allowing a nondestructive readout so that the process functions as a molecular optically controlled memory.